

Network Formation, Properties, and Actuation Performance of Functionalized Liquid Isoprene Rubber

Jishnu Nirmala Suresh,* Hans Liebscher, Hartmut Komber, Muhammad Tahir, Gerald Gerlach, and Sven Wießner



Cite This: *ACS Omega* 2024, 9, 4754–4761



Read Online

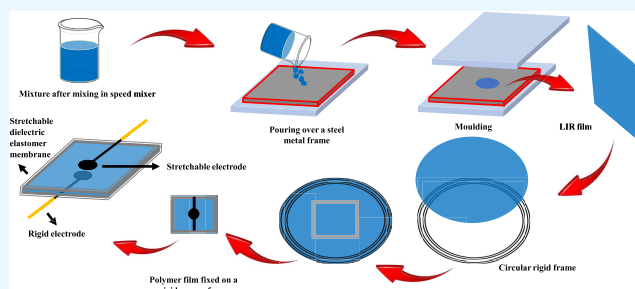
ACCESS |

Metrics & More

Article Recommendations

Supporting Information

ABSTRACT: Due to some useful mechanical, dynamic, and dielectric properties along with the ease of processing and forming, liquid rubbers are ideal materials for fabricating dielectric elastomer actuators in various configurations and for many potential applications ranging from automation to automobile and medical industry. In this study, we present a cross-linkable liquid rubber composition where amine-catalyzed esterification reactions lead to the formation of a network structure based on anhydride functional isoprene rubber, carboxyl-terminated nitrile-butadiene rubber, and epoxy end-capped prepolymers. The success of this intricate network formation procedure was verified by HR-MAS NMR spectroscopy. The new isoprene-based elastomeric material exhibits actuation-relevant attributes including a low elastic modulus of 0.45 MPa, soft response to an applied load up to a large deformation of 300%, and a dielectric constant value (2.6) higher than the conventional Elastosil silicone (2.2). A dot actuator comprising of an isoprene dielectric elastomer film in unstretched state and carbon paste electrodes was fabricated that demonstrated an electrode deformation of 0.63%, which is nearly twice as high as for the commercial Elastosil 2030 film (~0.30%) at 5 kV. Compared to the Elastosil silicone film, the enhanced performance is attributed to the low modulus and high dielectric constant value of the new isoprene elastomer.



The expansion–contraction characteristics of DEs are unique, which have been exploited in various studies in an attempt to develop soft actuators and robotic assemblies. Mostly, DEs such as silicone, acrylic, nitrile-butadiene rubber (NBR),^{11,12} hydrogenated nitrile-butadiene rubber (HNBR),^{6,13} carboxylated nitrile-butadiene rubber (XNBR),^{14,15} polyurethane,¹⁶ silicone rubber,^{17,18} etc., have been reported for potential applications as soft actuators.^{13,19–22} Among various dielectric elastomers, liquid rubbers offer benefits of fabrication ease, design flexibility, and compositional uniformity.^{23,24} Such characteristics also made liquid rubbers as attractive materials for emerging fabrication technologies such as the 3D printing process for fabricating DEAs in various geometric possibilities.^{25–29} The use of liquid rubbers is also advantageous for producing intricate structures such as adaptive fiber–elastomer composites with integrated actuators. Here, liquid rubbers can easily infiltrate into a woven textile structure without destroying the preferential orientations of fibers usually

1. INTRODUCTION

Electroactive polymers (EAPs) of ionic and electronic types are called “artificial muscles” and have attracted considerable research and innovation interest from the scientific community for soft robotic applications. The electronic EAPs such as dielectric elastomers (DEs) are important materials for soft actuators that exhibit large voltage-induced shape deformations, high elastic energy density, and fast responsiveness.^{1–4} Such exceptional properties made dielectric elastomer actuators (DEAs) appropriate for many fields of applications such as soft actuators, medical devices, automotive, aerospace, wearable technology, etc.^{5–7} A DEA comprises a flexible elastomer film sandwiched between two compliant electrodes. On applying voltage across opposing electrodes, a DE film contracts in thickness and expands in the plane direction, converting applied electrical energy into mechanical energy, which defines the actuation principle of a DEA. The strain S in thickness direction is defined by the following equation introduced by Pelrin et al.,⁸ where E is the electric field strength, Y the elastic modulus, ϵ the dielectric constant of the dielectric film, and ϵ_0 the dielectric constant of vacuum^{5,9,10}

$$S = \frac{\epsilon \epsilon_0 E^2}{Y}. \quad (1)$$

The expansion–contraction characteristics of DEs are unique, which have been exploited in various studies in an attempt to develop soft actuators and robotic assemblies. Mostly, DEs such as silicone, acrylic, nitrile-butadiene rubber (NBR),^{11,12} hydrogenated nitrile-butadiene rubber (HNBR),^{6,13} carboxylated nitrile-butadiene rubber (XNBR),^{14,15} polyurethane,¹⁶ silicone rubber,^{17,18} etc., have been reported for potential applications as soft actuators.^{13,19–22} Among various dielectric elastomers, liquid rubbers offer benefits of fabrication ease, design flexibility, and compositional uniformity.^{23,24} Such characteristics also made liquid rubbers as attractive materials for emerging fabrication technologies such as the 3D printing process for fabricating DEAs in various geometric possibilities.^{25–29} The use of liquid rubbers is also advantageous for producing intricate structures such as adaptive fiber–elastomer composites with integrated actuators. Here, liquid rubbers can easily infiltrate into a woven textile structure without destroying the preferential orientations of fibers usually

Received: October 13, 2023

Revised: December 5, 2023

Accepted: January 4, 2024

Published: January 18, 2024



desirable to achieve anisotropy in the composite physical properties.^{30–33}

Liquid silicone rubber has been widely investigated as a dielectric elastomer for fabricating simple to complex soft actuator/sensor structures.^{34–37} Although the silicone chemistry offers a versatile range of durable elastomers showing good relative permittivity and field-induced actuation, they naturally exhibit poor tear strength and abrasion resistance and thus are not the preferential choice for challenging environments and highly resilient applications.^{38–43} In order to address similar challenges and to develop novel materials for new and demanding applications of soft actuators, we report a new liquid rubber elastomer, which is electronically responsive with good overall performance characteristics.

Generally, isoprene elastomers are known for outstanding resilience, good resistance to tear and abrasion with a readily adaptable property profile by controlling the nature and density of cross-linked networks.^{44,45} In this work, a liquid isoprene rubber-based soft elastomeric material is developed, where a liquid cross-linker, comprising of an epoxy end-capped oligo(propylene oxide) and carboxy-terminated NBR (CNBR), was employed as a curative for liquid rubber. The developed formulation cured into a compositionally homogeneous elastomer like commercially available two-component liquid rubbers. However, herein, the epoxy cross-linker serves as a spacer chain for a flexible cross-linked network. Furthermore, the cross-linking reaction creates polar hydroxyl and carboxyl moieties, which contribute to improve the polarizability of newly developed soft elastomers.

To the best of our knowledge, no previous study has reported on the use of liquid isoprene rubber and the opted cross-linking chemistry to develop an electronically deformable elastomer for soft actuator applications.^{8,46–50}

2. MATERIALS AND METHODS

2.1. Materials. Commercially available liquid isoprene rubber (LIR-403, referred to as LIR in the manuscript) was purchased from Kuraray Europe GmbH (Hattersheim, Germany). LIR contains 93 mol % 1,4 units (*cis/trans* ratio ~ 70:30) and 7 mol % 3,4 units as determined by ¹H NMR spectroscopy (Figure S1a). LIR is grafted with three maleic anhydride units per molecule (34 000 g/mol) as reported in the supplier's data sheet. This corresponds to a degree of grafting of ~0.6 mol %. The presence of maleic anhydride groups could be identified in the ¹H NMR spectrum by signals of very low intensity in the range of 3.4–2.3 ppm (Figure S1a) and in the ¹³C NMR spectrum by carbonyl signals at 170.0 and 172.7 ppm (Figure S1b); however, they could not be quantified.

The liquid cross-linker (Struktol Polydis3616, Schill + Seilacher "Struktol" GmbH, Hamburg, Germany) is a mixture of carboxyl-terminated nitrile-butadiene rubber (CNBR) and low-molecular-weight glycidyl-terminated poly(propylene oxide) (epoxy-PPO). The composition of the CNBR was determined by ¹H NMR spectroscopy to be 29 mol % acrylonitrile, 59 mol % 1,4-butadiene, and 12 mol % 1,2-butadiene units (Figure S2a). The carboxylic groups could be identified in the ¹³C NMR spectrum but were not quantified (Figure S2b). Assuming an α,ω -bis(glycidyl)-termination, a degree of polymerization of 9 ($M_n \sim 600$ g/mol) was calculated for the epoxy-PPO from the ¹H NMR data (Figure S2a).

The catalyst 2,4,6-tris(dimethylaminomethyl)phenol (DMP-30) was purchased from Schill + Seilacher "Struktol" GmbH (Hamburg, Germany). The commercially available silicone film with a reported thickness of 200 μm (Elastosil 2030 film 250 mm/200 μm , WACKER, Munich, Germany) was also characterized for electromechanical actuation performance to highlight the actuation potentials of LIR. The formulation of the rubber mixture used for the fabrication of dot actuators is the following: liquid isoprene rubber (LIR-403) (100 phr), Struktol Polydis3616 (10 phr), and tris-(dimethylaminomethyl)phenol (DMP-30) (1 phr). This mixture and the final epoxy-cured material are denoted as C-LIR (compounded LIR).

2.2. Mixing and Molding Procedure. LIR is mixed with an epoxy cross-linker by using a SpeedMixer (DAC150 SP, Hauschild GmbH & Co. KG, Hamm, Germany). The mixing ingredients were weighed in a PP container and subjected to the following mixing sequence [rotational speed (time)]: 800 rpm (5 s), 2500 rpm (120 s), 1200 rpm (5 s), 2500 rpm (100 s), 800 rpm (5 s). This mixing sequence was repeated three times. The cross-linking behavior of liquid rubber mixtures was characterized at 160 °C by using an oscillating shear curemeter (SIS V-50, Scarabaeus Mess-und Produktionstechnik GmbH, Wetzlar, Germany). The cure characteristics were obtained from the curing profile and used to vulcanize the liquid rubber composition into C-LIR elastomers by using a hotpress (TP 1000, Fontijne Presses, Delft, The Netherlands).

2.3. Extraction and Swelling Experiments. In addition to the NMR structure investigation, we conducted distinct swelling and extraction experiments. These experiments aimed to determine the amount and composition of the soluble fraction that remains, including the residual uncross-linked LIR, leftover epoxy curing agent, and CNBR component. This information was crucial in elucidating the intricate network formation process. A small piece of the cured material ($\sim 10 \times 10 \times 2$ mm³) was placed in a vial and 5 mL of chloroform was added. The vial was placed on a circular vibrating shaker Vibramax 100 (Heidolph Instruments GmbH & Co. KG, Schwabach, Germany) at 300 rpm for 2 h. Then, the first extract was removed and after addition of 5 mL of chloroform again, the material was further extracted at 300 rpm for 20 h. From the weight before extraction, the weight of the swollen material after removing the second extract, and the weight of the vacuum-dried material after extraction, the solvent uptake (density (CHCl₃) = 1.49 g/mL) and the weight loss due to extraction were calculated.

3. CHARACTERIZATION TECHNIQUES

3.1. Structural Characterization. NMR spectra were recorded on a Bruker Advance III 500 spectrometer (Bruker, Ettlingen, Germany) operating at 500.13 MHz for ¹H and at 125.76 MHz for ¹³C at 30 °C. The spectra were referenced to the solvent signal (CDCl₃: $\delta(^1\text{H}) = 7.26$ ppm; $\delta(^{13}\text{C}) = 77.0$ ppm). For high-resolution magic angle spinning (HR-MAS) measurements, the PTFE insert of the ZrO₂ rotor (4 mm outer diameter, 50 μL insert volume) was filled with small pieces of the material (~ 2 mg). After the addition of CDCl₃ and 30 min swelling time, the sample was measured with a HR-MAS probe (Bruker, Germany) at $\nu_r = 4000$ Hz.

3.2. Tensile and Dynamic-Mechanical Characterization. The tensile test of the sample is conducted according to the standard DIN 53504 using a Universal Testing Machine (UTM) Zwick 1456, Z010 (ZwickRoell GmbH & Co. KG

Ulm, Germany) equipped with optical strain sensors and a 1 kN force transducer at a crosshead speed of 200 mm/min by using S2-type dog bone shaped specimen which were punched out of the compression molded vulcanized sheets. From the tests, the stress–strain curves as well as average values of stress at break and strain at break were obtained.

The temperature-dependent dynamic-mechanical behavior of the elastomers was characterized by temperature sweeps on a GABO EPLEXOR 150N (Gabo Qualimeter GmbH, Ahlden, Germany) using rectangular specimens with sample dimensions of 35 mm × 10 mm, which were punched out from the 2-mm-thick plate using specific dies. The tests were carried out in tension mode at a prestrain of 2% and a dynamic strain of 0.5%, 2 K/min heating rate, and in the temperature range of –120 to 100 °C.

3.3. Dielectric Characterization. The dielectric properties of the samples were analyzed at 23 °C in the frequency range from 1 Hz to 1 MHz by impedance spectroscopy using a Solartron SI 1260A frequency response analyzer with the 1296A interface system and a 12962A sample holder (Solartron Analytical U.K., Farnborough, U.K.). Circular disc-shaped elastomer samples with a diameter of 25 mm were clamped between the electrodes of the sample holder. From the real and imaginary parts of impedance Z , the capacitance of the sample holder with the inserted elastomer sample C_{sample} was calculated.⁵⁰ Subsequently, the empty sample holder was measured in air, whereby the electrode distance was set to the same value as that before with the respective elastomer sample inserted. Also, for the empty configuration, the capacitance $C_{\text{empty cell}}$ was derived. The relative dielectric constant ϵ_r was then calculated according to DIN EN 62631-1:2012-03:

$$\epsilon_r = \frac{C_{\text{sample}}(f)}{C_{\text{empty cell}}(f)} \quad (2)$$

3.4. DEA Deformation Measurements. Both C-LIR and Elastosil films were bonded, without prestretching, onto an acrylic frame by using a double-sided adhesive tape—Adhesive Research EL-8932EE (Adhesive Research Inc., Glen Rock, PA, USA). In order to correlate electrode deformation with the electric field strength, we measured the film thickness at the electrode region before applying carbon paste electrodes. An incremental probe (IKF 10, Feinmess Suhl GmbH, Germany) with a plate-shaped measuring insert of 4 mm diameter and a display unit (PU 11, Feinmess Suhl GmbH, Germany) was used for thickness measurements. About eight measuring values were recorded, giving average thicknesses of 248 and 185 μm for C-LIR and Elastosil films, respectively.

Both sides of the dielectric elastomer film were coated with concentric circular electrodes of conductive carbon paste (Gelest ExSil50 mixed with 11 phr Printex XE2B) by using adhesive stencils 50 mm in diameter with a 3-mm-wide connecting strip extending from the electrodes to the acrylic frame. The connection strips were attached to the copper adhesive tape, which connects to the high-voltage power supply (Peta-pico-Voltron). The experimental setup for measuring the actuator deformation is shown in Figure 1.

DEAs were actuated by applying a voltage ranging from 0 to 5000 V, corresponding to the device's maximum operational voltage. The voltage was incremented in 500 V intervals, and during each step, the corresponding radial electrode strain was recorded. A compact camera (Sony α 6400) with a macro lens

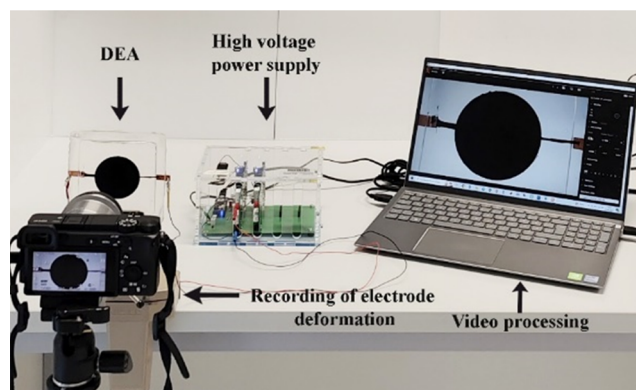


Figure 1. Measurement setup for DEA deformation.

(Sony SEL30M35) was employed for video capture at a speed of 100 frames/s by setting a 12.5 cm distance between the lens and the observed electrode. The electrode strain is extracted by video processing using MATLAB and the proportional increase in electrode area upon actuation is considered as an ideal circular surface.

The components of rubber formulation, methods of mixing and rheology, elastomer production, and characterization techniques are summarized in the block flow diagram of Figure 2.

4. RESULTS AND DISCUSSION

4.1. Curing Characteristics. The cross-linking behavior of C-LIR is measured at 160 °C by using an oscillating shear curemeter and plotted as a torque-versus-time response in Figure 3. The rubber mixture was squeezed in a biconical die assembly preheated under a constant temperature of 160 °C to run a time sweep test at a fixed standard frequency and deformation amplitude. The torque value increases over time showing epoxy–anhydride esterification reactions between epoxy end-capped PPO short chains and anhydride functional isoprene rubber and thus forming poly(propylene oxide) flexible bridges (PPO) between rubber chains. The torque value increases and tends to stabilize, reflecting the establishment of a cross-linked rubber network. After 60 min, the C-LIR reveals a maximum torque value of 1.6 dNm, which is used to determine the optimum cure time for the compression molding process. In comparison to solid isoprene rubber, which typically possesses a molecular weight range of approximately 300,000–1,000,000 g/mol,⁵¹ the torque exhibited by C-LIR is significantly low due to its lower molecular mass of 35 000 g/mol and merely three anhydride groups per molecule.

4.2. Network Formation. The network formation is based on the reaction of the anhydride groups of the functionalized IR and the carboxyl groups of the CNBR, with the epoxide groups of epoxy-PPO catalyzed by 2,4,6-tris-(dimethylaminomethyl)phenol.^{52–54} Following these esterification reactions, subsequent reactions can take place (esterification, transesterification, and ether formation), leading to a structurally complex network (Scheme S1). While individual reactions cannot be followed in detail, a combination of NMR structure investigations and extraction experiments was used to derive conclusions on network formation.

Figure 4a shows the ¹H NMR spectrum of the mixture before addition of the catalyst. Despite considerable signal

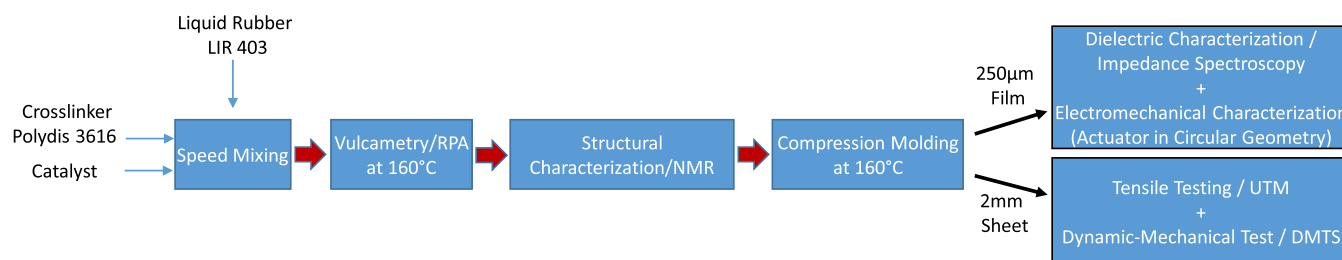


Figure 2. Schematic illustration of materials, methods, and characterization techniques used in the present work.

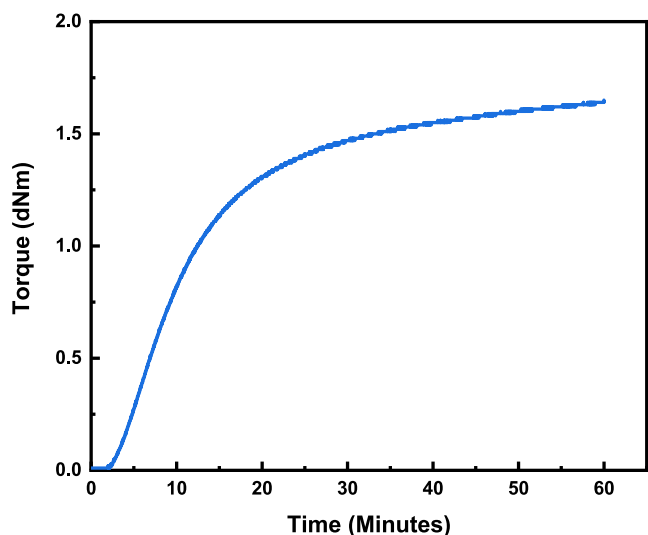


Figure 3. Curing profile of C-LIR at 160 °C.

overlap, several signal regions are characteristic of the different components of the mixture. The range 5.8–5.3 ppm represents the $-\text{CH}=\text{}$ signals of the 1,2- and 1,4-butadiene units of the CNBR. The signals in the range 5.3–4.9 ppm are from both the $=\text{CH}_2$ protons of the 1,2-butadiene units of CNBR and the $-\text{CH}=\text{}$ signals of the 1,4 units of IR. The corresponding

$=\text{CH}_2$ protons of the 3,4 units of the IR give the signal groups between 4.8 and 4.6 ppm. The signals in the range of 4.2–3.2 ppm are from the OCH and OCH₂ protons of epoxy-PPO with the CH₃ signal at \sim 1.15 ppm. Finally, the epoxy group can be identified by the signals at 3.13, 2.78, and 2.61 ppm.

While the reaction mixture could be studied as a solution in CDCl₃, the cross-linked material is no longer soluble and was studied as a gel swollen with CDCl₃ using high-resolution magic angle spinning (HR-MAS) NMR spectroscopy.⁵⁵ Figure 4b shows the ¹H HR-MAS spectrum after network formation. The signals of the epoxy groups almost completely disappeared, indicating suitable curing conditions. An experimental detection of the formed ester and ether groups is not possible because the new signals are of low intensity and also strongly broadened, as they represent the network point with limited mobility. The material was extracted with chloroform, and the extractable fraction was determined to be about 12 wt %. Comparing the ¹H NMR spectra of extracted (Figure 4c) and nonextracted materials (Figure 4a), the lower content of NBR and PPO in the extracted material is obvious.

The ¹H NMR spectrum of the extract (Figure S3) shows that the extracted PPO is mainly nonfunctionalized and thus nonreactive. The higher extractability of CNBR compared to IR indicates a lower reactivity of the terminal COOH groups compared to the anhydride groups of IR and probably also a content of nonfunctionalized NBR. The solvent uptake is 10.3

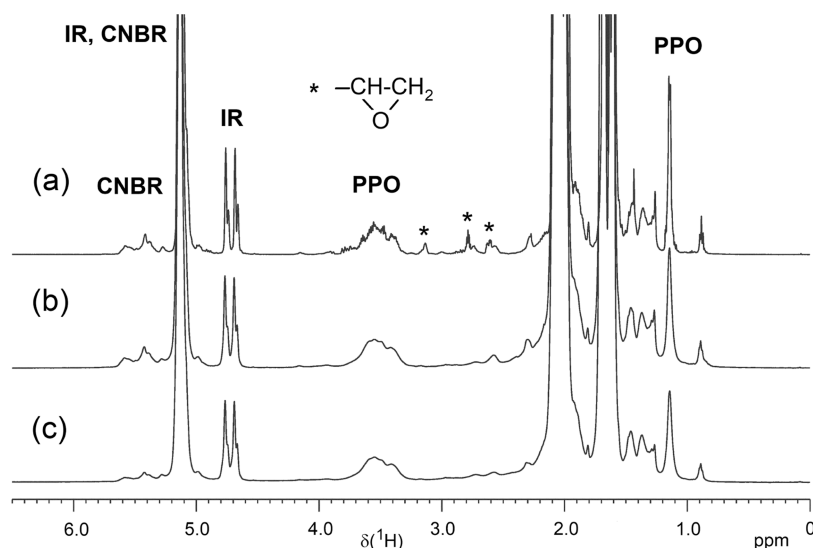


Figure 4. ¹H NMR spectra of (a) reaction mixture of C-LIR without catalyst (asterisks mark signals of the epoxy group), (b) cross-linked material C-LIR, and (c) C-LIR after extraction with chloroform. Spectrum (a) was measured as solution in CDCl₃, whereas spectra (b, c) are ¹H HR-MAS spectra recorded from samples swollen with CDCl₃. For better comparability, the spectra are referenced to the same integral intensity of the signals in the range 4.9–4.6 ppm ($=\text{CH}_2$ protons of the 3,4 units of the IR).

mL/g for the extracted sample, which represents quite good swelling and indicates a loose network.

4.3. Tensile Test Results. The ability of a dielectric elastomer to undergo large voltage-induced deformations is an important requirement. Therefore, the tensile testing of the isoprene elastomer was performed to find out its load–deformation behavior (see Figure 5). C-LIR demonstrates a

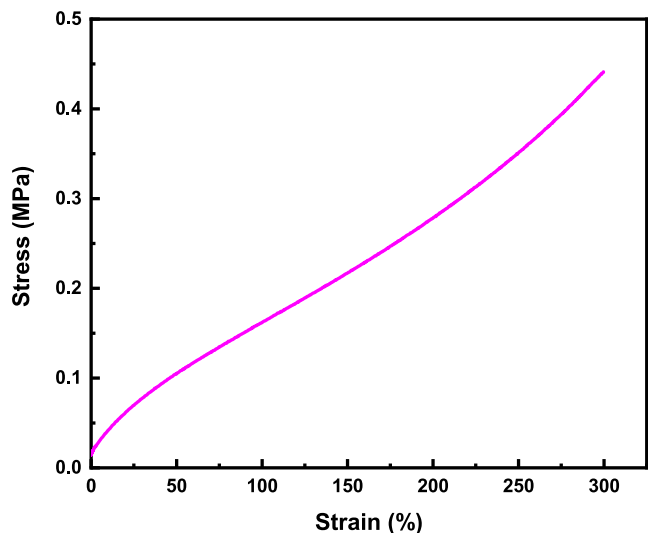


Figure 5. Stress–strain curve of C-LIR.

low modulus response to an applied load up to a large deformation of 300% strain at break. The high strain value of C-LIR indicates large attainable prestretching levels and the ability to undergo large-strain actuations before rupturing. Advantageously, C-LIR exhibits a low elastic modulus value of 0.45 MPa, which is an important performance parameter according to eq 1, i.e., the lower the modulus is, the higher is the voltage-induced strain of a dielectric elastomer.

The tensile strength of the soft isoprene elastomer is very low at 0.43 MPa for 300% strain. This enables the isoprene

elastomer to attain a desirable actuation level at low applied voltage and Maxwell stresses, which is advantageous for soft actuator technology.

4.4. Dynamic-Mechanical Analysis. To analyze the temperature-dependent viscoelastic behavior and to determine the glass transition temperature (indicating segmental relaxation process) of C-LIR, a temperature-sweep dynamic-mechanical measurement was performed. The measurement data, plotted in Figure 6, identifies the glass transition temperature of C-LIR at $-47\text{ }^{\circ}\text{C}$, which highlights its applicability in subzero actuation and robotics applications. The storage modulus of C-LIR is low, approximately $\sim 2\text{ MPa}$, indicating its low dynamic stiffness. C-LIR possesses viscoelastic properties of a resilient elastomer (low $\tan \delta$) at temperatures beyond the glass transition temperature and in the rubbery plateau region, which is a crucial parameter in actuator performance for its fast and reversible response (Figure 7).

4.5. Dielectric Properties. The evaluation of the dielectric properties of the elastomers was done in the frequency range of 1 Hz to 1 MHz. The dielectric response of C-LIR and Elastosil as a function of frequency is plotted in Figure 8. It can be seen that the dielectric constant ϵ_r of C-LIR is higher than the ϵ_r of Elastosil across the whole measured frequency range. It gradually decreases with increasing frequency for C-LIR, while it remains nearly constant for Elastosil in the measuring frequency range from 1 to 10^6 Hz . In particular, C-LIR exhibits a relative dielectric constant of 2.6 as compared to the value of 2.2 for Elastosil at a frequency of 10 Hz.

C-LIR shows a distinct dielectric loss peak, which indicates high dissipation of electrical energy owing to the presence of polarizing species with a relaxation peak at around 10^3 Hz . The use of the epoxy–anhydride cross-linking mechanism produces polar species with polarization mechanisms that interact with the applied field for high dielectric losses in C-LIR. On the contrary, the polarization mechanism in Elastosil adjusts with the switching electric field (AC oscillations) and shows minimal dissipation of electrical energy.

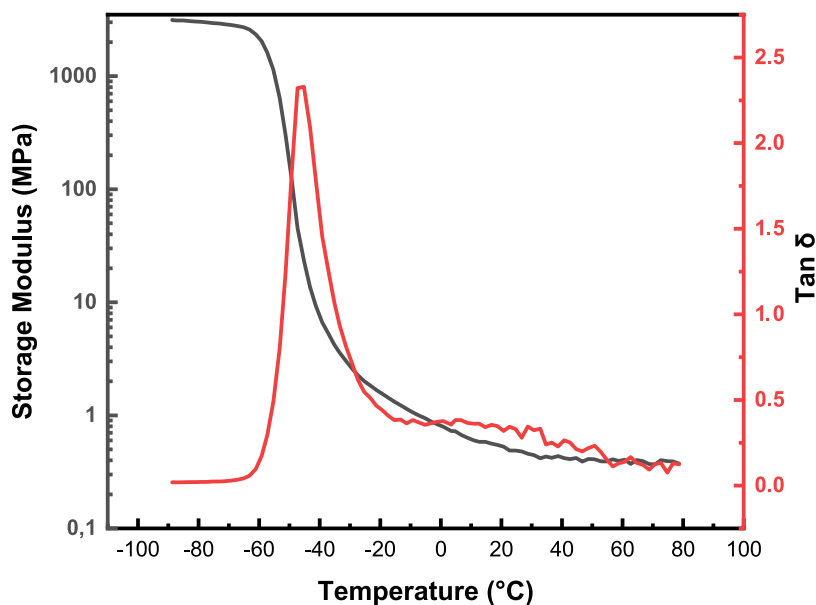


Figure 6. Storage modulus (black color) and mechanical loss factor (red color) vs temperature curves of C-LIR.

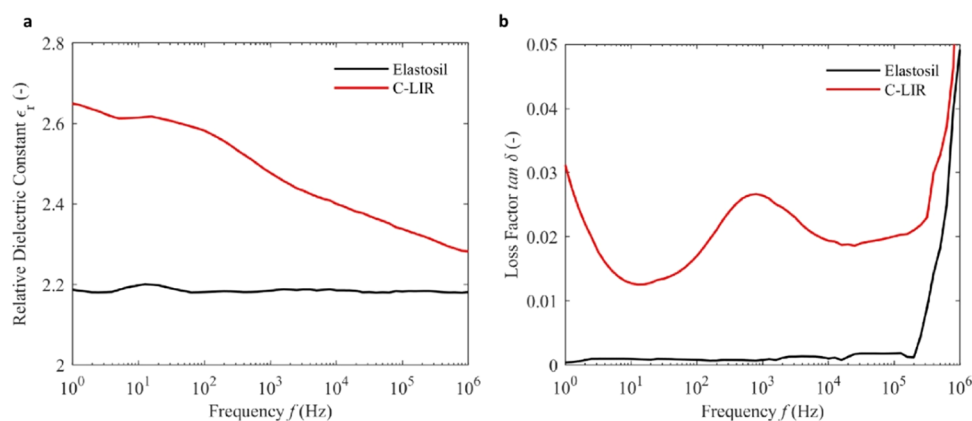


Figure 7. (a) Frequency-dependent relative dielectric constant and (b) dielectric loss of C-LIR (thickness: 248 μm) and Elastosil film (thickness: 185 μm).

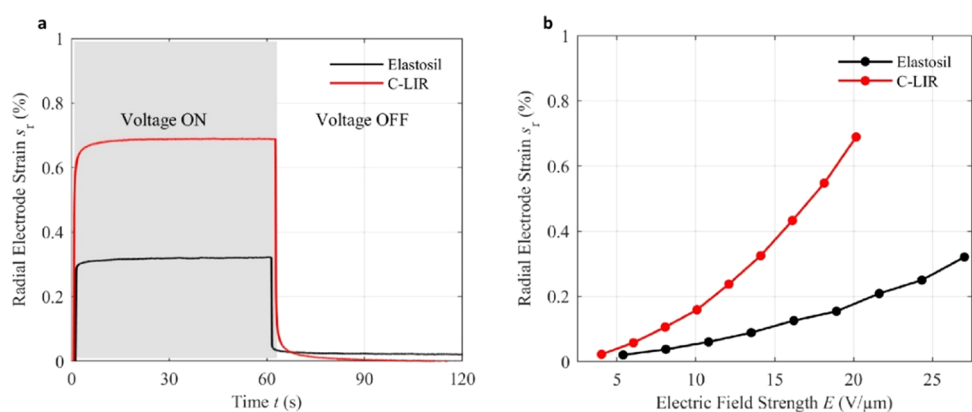


Figure 8. Voltage-induced radial strain of C-LIR and Elastosil films without prestretching: (a) Time-dependent electrode strain of planar dot actuators at a constant voltage level of 5 kV applied for 60 s and (b) electric-field-dependent electrode strain of planar dot actuators.

Table 1. Measured Values of Dielectric Constant and Tensile Properties of C-LIR and the Elastosil 2030 Film

	dielectric constant	elastic modulus (MPa)	tensile strength (MPa)	elongation at break (%)
C-LIR	2.6	0.45 ± 0.03	0.43 ± 0.03	300 ± 40
Elastosil 2030 film	2.2	1.51 ± 0.06	9.55 ± 0.98	574 ± 20

The dielectric and tensile properties of C-LIR and the Elastosil film are summarized in Table 1. The increase in the dielectric constant value of C-LIR over Elastosil is advantageous for enhanced actuation strains at low field strengths. Also, due to large tensile deformations at much lower stress values, the C-LIR elastomer is easy to prestretch by applying small tensile loads and is actuated for relatively large deformations by Maxwell stresses of low magnitude as compared to Elastosil.

4.6. DEA Deformation Measurements. The time-dependent radial strain of the actuator electrode at an operating voltage of 5 kV is exemplarily shown in Figure 8a. Both elastomers show a rectangular-shaped square wave response in electrode strain, which indicates a fast response with low time constants. It should be noted that C-LIR actuators exhibit a larger radial electrode strain (0.63%) compared to Elastosil actuators (0.30%) even with an approximately 60- μm -thick C-LIR film. This is due to the inherently higher dielectric constant and lower elastic modulus value of C-LIR.

The voltage applied across the dielectric elastomer is gradually increased from 0 to 5 kV and then the steady

actuation strain is measured and plotted in Figure 8b. It can be seen that the electrically actuated strain of C-LIR is larger than that of Elastosil at low and high field strengths. Notably, even though the thickness of the C-LIR film (248 μm) is higher than that of the Elastosil film (185 μm), its electromechanical performance exceeded in actuated strain.

5. CONCLUSIONS

A cross-linkable liquid rubber composition comprising of isoprene rubber and epoxy end-capped low-molecular-weight PPO and CNBR molecules was developed and comprehensively characterized. The cross-linking of rubber chains through epoxy - anhydride/carboxylic acid curing chemistry was evident by rheology test and the details of structure and network formations were confirmed by NMR measurements. The esterification reaction between rubbers and cross-linker produces polar moieties (hydroxy, ester, carboxylic), which enhance the electric-field-induced polarizability of isoprene elastomer. The tensile testing of C-LIR demonstrates soft response to an applied load up to a large deformation, and the dynamic-mechanical testing shows its low dynamic stiffness and resilient response for soft actuator applications. The

relative permittivity of C-LIR and the electromechanical actuation of its circular actuator are improved when compared with the commercial Elastosil 2030 silicone film.

All in all, the newly developed isoprene dielectric elastomer is soft, resilient, adaptable (wide range of stiffnesses and strains are possible by network adjustments), and possesses a relative permittivity value higher than silicone, which makes C-LIR an attractive elastomer for soft actuators and robotics applications.

■ ASSOCIATED CONTENT

SI Supporting Information

The Supporting Information is available free of charge at <https://pubs.acs.org/doi/10.1021/acsomega.3c08022>.

¹H and ¹³C NMR spectra of LIR and Polydis3616; ¹H NMR spectra of the reaction mixture of C-LIR and of the chloroform extract obtained after curing; and overview of main reactions occurring during curing in epoxide–anhydride–acid systems (PDF)

■ AUTHOR INFORMATION

Corresponding Author

Jishnu Nirmala Suresh – Institute of Materials Science, Faculty of Mechanical Science and Engineering, Dresden University of Technology, 01062 Dresden, Germany; Research Division Elastomers, Leibniz-Institut für Polymerforschung Dresden e.V., 01069 Dresden, Germany; orcid.org/0000-0002-2624-2855; Email: nirmala@ipfdd.de

Authors

Hans Liebscher – Institute of Solid-State Electronics, Faculty of Electrical and Computer Engineering, Dresden University of Technology, 01062 Dresden, Germany

Hartmut Komber – Center Macromolecular Structure Analysis, Leibniz-Institut für Polymerforschung Dresden e.V., 01069 Dresden, Germany; orcid.org/0000-0001-6176-6737

Muhammad Tahir – Research Division Elastomers, Leibniz-Institut für Polymerforschung Dresden e.V., 01069 Dresden, Germany

Gerald Gerlach – Institute of Solid-State Electronics, Faculty of Electrical and Computer Engineering, Dresden University of Technology, 01062 Dresden, Germany

Sven Wießner – Institute of Materials Science, Faculty of Mechanical Science and Engineering, Dresden University of Technology, 01062 Dresden, Germany; Research Division Elastomers, Leibniz-Institut für Polymerforschung Dresden e.V., 01069 Dresden, Germany; orcid.org/0000-0003-0967-4557

Complete contact information is available at: <https://pubs.acs.org/10.1021/acsomega.3c08022>

Notes

The authors declare no competing financial interest.

■ ACKNOWLEDGMENTS

The research was funded by the Deutsche Forschungsgemeinschaft (DFG, German Research Foundation) – GRK 2430 – 380321452 within the research training group "Interactive Fiber-Rubber Composites". The authors express their appreciation to Andreas Korwitz for performing the swelling and extraction experiments as well as to Holger Scheibner for

conducting the tensile testing (both from IPF Dresden). Furthermore, the authors acknowledge Kuraray Europe GmbH for their kind support in providing the LIR essential to the research endeavors.

■ REFERENCES

- (1) Liebscher, H.; Tahir, M.; Wiessner, S.; Gerlach, G. Effect of barium titanate particle filler on the performance of polyurethane-based dielectric elastomer actuators. In *Electroactive Polymer Actuators and Devices (EAPAD) XXIV*; SPIE, 2022; p 12042 DOI: [10.1117/12.2612354](https://doi.org/10.1117/12.2612354).
- (2) Wang, K.; Ouyang, G.; Chen, X.; Jakobsen, H. Engineering Electroactive Dielectric Elastomers for Miniature Electromechanical Transducers. *Polym. Rev.* **2017**, *57*, 369–396.
- (3) Guo, Y.; Qin, Q.; Han, Z.; Plamthottam, R.; Possinger, M.; Pei, Q. Dielectric elastomer artificial muscle materials advancement and soft robotic applications. *SmartMat* **2023**, *4*, No. e1203.
- (4) Gu, G.-Y.; Gupta, U.; Zhu, J.; Zhu, L.-M.; Zhu, X.-Y. Feedforward deformation control of a dielectric elastomer actuator based on a nonlinear dynamic model. *Appl. Phys. Lett.* **2015**, *107*, No. 042907.
- (5) Suresh, J. N.; Arief, I.; Naskar, K.; Heinrich, G.; Tahir, M.; Wießner, S.; et al. The role of chemical microstructures and compositions on the actuation performance of dielectric elastomers: A materials research perspective. *Nano Sel.* **2023**, *4*, 289–315.
- (6) Yang, D.; Tian, M.; Li, D.; Wang, W.; Ge, F.; Zhang, L. Enhanced dielectric properties and actuated strain of elastomer composites with dopamine-induced surface functionalization. *J. Mater. Chem. A* **2013**, *1*, 12276–12284.
- (7) Tian, M.; Ma, Q.; Li, X.; Zhang, L.; Nishi, T.; Ning, N. High performance dielectric composites by latex compounding of graphene oxide-encapsulated carbon nanosphere hybrids with XNBR. *J. Mater. Chem. A* **2014**, *2*, 11144–11154.
- (8) Pelrine, R. E.; Kornbluh, R. D.; Joseph, J. P. Electrostriction of polymer dielectrics with compliant electrodes as a means of actuation. *Sens. Actuators, A* **1998**, *64*, 77–85.
- (9) Zhang, L.; Wang, D.; Hu, P.; Zha, J. W.; You, F.; Li, S. T.; et al. Highly improved electro-actuation of dielectric elastomers by molecular grafting of azobenzenes to silicon rubber. *J. Mater. Chem. C* **2015**, *3*, 4883–4889.
- (10) Ning, N.; Ma, Q.; Liu, S.; Tian, M.; Zhang, L.; Nishi, T. Tailoring Dielectric and Actuated Properties of Elastomer Composites by Bioinspired Poly(dopamine) Encapsulated Graphene Oxide. *ACS Appl. Mater. Interfaces* **2015**, *7*, 10755–10762.
- (11) Gunasekaran, S.; Natarajan, R. K.; Kala, A.; Jagannathan, R. Dielectric studies of some rubber materials at microwave frequencies. *Indian J. Pure Appl. Phys.* **2008**, *46*, 733–737.
- (12) Yang, D.; Kong, X.; Ni, Y.; Gao, D.; Yang, B.; Zhu, Y.; et al. Novel nitrile-butadiene rubber composites with enhanced thermal conductivity and high dielectric constant. *Composites, Part A* **2019**, *124*, No. 105447.
- (13) Yang, D.; Tian, M.; Dong, Y.; Liu, H.; Yu, Y.; Zhang, L. Disclosed dielectric and electromechanical properties of hydrogenated nitrile-butadiene dielectric elastomer. *Smart Mater. Struct.* **2012**, *21*, No. 035017.
- (14) Yang, D.; Ni, Y.; Kong, X.; Xue, H.; Guo, W.; Zhang, L. Enhanced electromechanical properties of natural rubber using highly efficient and cost-effective mussel-inspired modification of TiO₂ nanoparticles. *Appl. Surf. Sci.* **2019**, *495*, No. 143638.
- (15) Yang, D.; Yu, L.; Liang, Y.; Wei, Q.; Ni, Y.; Zhang, L. Enhanced Electromechanical Performance of Natural Rubber Composites via Constructing Strawberry-like Dielectric Nanoparticles. *ACS Appl. Polym. Mater.* **2020**, *2*, No. 5621.
- (16) Yang, Y.; Gao, Z.-S.; Yang, M.; Zheng, M.-S.; Wang, D.-R.; Zha, J.-W.; et al. Enhanced energy conversion efficiency in the surface modified BaTiO₃ nanoparticles/polyurethane nanocomposites for potential dielectric elastomer generators. *Nano Energy* **2019**, *59*, 363–371.

- (17) Jiang, L.; Betts, A.; Kennedy, D.; Jerrams, S. Improving the electromechanical performance of dielectric elastomers using silicone rubber and dopamine coated barium titanate. *Mater. Des* **2015**, *85*, 733–742.
- (18) Gale, C. B.; Brook, M. A.; Skov, A. L. Compatibilization of porphyrins for use as high permittivity fillers in low voltage actuating silicone dielectric elastomers. *RSC Adv.* **2020**, *10*, 18477–18486.
- (19) Yin, Q.; Wen, Y.; Jia, H.; Hong, L.; Ji, Q.; Xu, Z. Enhanced mechanical, dielectric, electrical and thermal conductive properties of HXNBR/HNBR blends filled with ionic liquid-modified multiwalled carbon nanotubes. *J. Mater. Sci.* **2017**, *52*, 10814–10828.
- (20) Yang, D.; Zhang, L.; Ning, N.; Li, D.; Wang, Z.; Nishi, T.; et al. Large increase in actuated strain of HNBR dielectric elastomer by controlling molecular interaction and dielectric filler network. *RSC Adv.* **2013**, *3*, 21896.
- (21) WANG, Y.; SUO, J.; WANG, D.; WEI, L.; HOU, P.; PAN, J.; et al. Oriented molybdenum disulfide-silica/hydrogenated nitrile butadiene rubber composites: Effects of nanosheets on mechanical and dielectric properties. *Chin. J. Aeronaut.* **2023**, *36*, 413–422.
- (22) Yang, D.; Tian, M.; Dong, Y.; Liu, H.; Yu, Y.; Zhang, L. Disclosed dielectric and electromechanical properties of hydrogenated nitrile-butadiene dielectric elastomer. *Smart Mater. Struct.* **2012**, *21*, No. 035017.
- (23) Brochu, P.; Pei, Q. Advances in Dielectric Elastomers for Actuators and Artificial Muscles. *Macromol. Rapid Commun.* **2010**, *31*, 10–36.
- (24) Carpi, F.; de Rossi, D.; Kornbluh, R.; Pelrine, R.; Sommer-Larsen, P. *Dielectric Elastomers as Electromechanical Transducers: Fundamentals, Materials, Devices, Models and Application of an Emerging Electroactive Polymer Technology*; Elsevier, 2010.
- (25) Martinez, R. V.; Branch, J. L.; Fish, C. R.; Jin, L.; Shepherd, R. F.; Nunes, R. M. D.; et al. Robotic Tentacles with Three-Dimensional Mobility Based on Flexible Elastomers. *Adv. Mater.* **2013**, *25*, 205–212.
- (26) Chen, T.; Bilal, O. R.; Shea, K.; Daraio, C. Harnessing bistability for directional propulsion of soft, untethered robots. *Proc. Natl. Acad. Sci.* **2018**, *115*, 5698–5702.
- (27) Yuk, H.; Lu, B.; Lin, S.; Qu, K.; Xu, J.; Luo, J.; et al. 3D printing of conducting polymers. *Nat. Commun.* **2020**, *11*, No. 1604.
- (28) Tolley, M. T.; Felton, S. M.; Miyashita, S.; Xu, L.; Rus, D.; Zhou, M. et al. *Self-folding shape memory laminates for automated fabrication*, IEEE/RSJ International Conference on Intelligent Robots and Systems; IEEE: 2013; 4931–4936.
- (29) Muth, J. T.; Vogt, D. M.; Truby, R. L.; Mengüç, Y.; Kolesky, D. B.; Wood, R. J.; et al. Embedded 3D Printing of Strain Sensors within Highly Stretchable Elastomers. *Adv. Mater.* **2014**, *26*, 6307–6312.
- (30) Kaynak, C.; Arikan, A.; Tincer, T. Flexibility improvement of short glass fiber reinforced epoxy by using a liquid elastomer. *Polymer* **2003**, *44*, 2433–2439.
- (31) Chortos, A.; Hajiesmaili, E.; Morales, J.; Clarke, D. R.; Lewis, J. A. 3D Printing of Interdigitated Dielectric Elastomer Actuators. *Adv. Funct. Mater.* **2020**, *30*, No. 1907375.
- (32) Rossiter, J.; Walters, P.; Stoimenov, B. *Printing 3D dielectric elastomer actuators for soft robotics*, *Electroact. Polym. Actuators Devices*, 200972870H DOI: [10.1117/12.815746](https://doi.org/10.1117/12.815746).
- (33) Palmić, T. B.; Slavič, J. Single-process 3D-printed stacked dielectric actuator. *Int. J. Mech. Sci.* **2022**, *230*, No. 107555.
- (34) Shit, S. C.; Shah, P. A Review on Silicone Rubber. *Natl. Acad. Sci. Lett.* **2013**, *36*, 355–365.
- (35) Zhang, W.; Li, X.; Shan, Z.; Wang, S.; Xiao, Y. Surface modification of magnesium hydroxide by wet process and effect on the thermal stability of silicone rubber. *Appl. Surf. Sci.* **2019**, *465*, 740–746.
- (36) Lehretz, F.; Krebler, J.; Nase, M.; Rennert, M.; Schulte-Fischedick, J.; Seifert, J. M. Enhancement of Acid Stability of Silicone Elastomers by Using Inert Fillers. *IEEE Trans. Dielectr. Electr. Insul.* **2020**, *27*, 2188–2194.
- (37) Farhadinejad, Z.; Ehsani, M.; Ahmadi-Joneidi, I.; Shayegani, A.; Mohseni, H. Effects of UVC radiation on thermal, electrical and morphological behavior of silicone rubber insulators. *IEEE Trans. Dielectr. Electr. Insul.* **2012**, *19*, 1740–1749.
- (38) Huang, P.; Xia, Z.; Cui, S. 3D printing of carbon fiber-filled conductive silicon rubber. *Mater. Des* **2018**, *142*, 11–21.
- (39) Chen, Q.; Zhao, J.; Ren, J.; Rong, L.; Cao, P.; Advincula, R. C. 3D Printed Multifunctional, Hyperelastic Silicone Rubber Foam. *Adv. Funct. Mater.* **2019**, *29*, No. 1900469.
- (40) Hajash, K.; Sparrman, B.; Guberan, C.; Laucks, J.; Tibbits, S. Large-Scale Rapid Liquid Printing. *3D Print. Addit. Manuf.* **2017**, *4*, 123–132.
- (41) Zheng, R.; Chen, Y.; Chi, H.; Qiu, H.; Xue, H.; Bai, H. 3D Printing of a Polydimethylsiloxane/Polytetrafluoroethylene Composite Elastomer and its Application in a Triboelectric Nanogenerator. *ACS Appl. Mater. Interfaces* **2020**, *12*, 57441–57449.
- (42) Foerster, A.; Annarasa, V.; Terry, A.; Wildman, R.; Hague, R.; Irvine, D.; et al. UV-curable silicone materials with tuneable mechanical properties for 3D printing. *Mater. Des* **2021**, *205*, No. 109681.
- (43) Giffney, T.; Bejanin, E.; Kurian, A. S.; Travas-Sejdic, J.; Aw, K. Highly stretchable printed strain sensors using multi-walled carbon nanotube/silicone rubber composites. *Sens. Actuators, A* **2017**, *259*, 44–49.
- (44) Imai, K. United States Patent (19) 1988.
- (45) Kamble, V. G.; Mersch, J.; Tahir, M.; Stöckelhuber, K. W.; Das, A.; Wießner, S. Development of Liquid Diene Rubber Based Highly Deformable Interactive Fiber-Elastomer Composites. *Materials* **2022**, *15*, 390.
- (46) Novelli, G. L.; Vargas, G. G.; Andrade, R. M. Dielectric elastomer actuators as artificial muscles for wearable robots. *J. Intell. Mater. Syst. Struct.* **2023**, *34*, 1007–1025.
- (47) Sheima, Y.; Venkatesan, T. R.; Frauenrath, H.; Opris, D. M. Synthesis of polysiloxane elastomers modified with sulfonyl side groups and their electromechanical response. *J. Mater. Chem. C* **2023**, *11*, 7367–7376.
- (48) Xiong, L.; Li, D.; Yang, Y.; Ye, X.; Huang, Y.; Xu, E.; et al. Tailoring crosslinking networks to fabricate photocurable polyurethane acrylate (PUA) dielectric elastomer with balanced electromechanical performance. *React. Funct. Polym.* **2023**, *183*, No. 105498.
- (49) Youn, J.-H.; Jeong, S. M.; Hwang, G.; Kim, H.; Hyeon, K.; Park, J.; et al. Dielectric Elastomer Actuator for Soft Robotics Applications and Challenges. *Appl. Sci.* **2020**, *10*, 640.
- (50) Sahu, D.; Sahu, R. K.; Patra, K. In-plane actuation performance of graphene oxide filled VHB 4910 dielectric elastomer. *J. Appl. Polym. Sci.* **2022**, *139*, No. 51594.
- (51) Sriring, M.; Nimpaiboon, A.; Kumarn, S.; Sirisinha, C.; Sakkapipanich, J.; Toki, S. Viscoelastic and mechanical properties of large- and small-particle natural rubber before and after vulcanization. *Polym. Test* **2018**, *70*, 127–134.
- (52) Yang, T.; Zhang, C.; Zhang, J.; Cheng, J. The influence of tertiary amine accelerators on the curing behaviors of epoxy/anhydride systems. *Thermochim. Acta* **2014**, *577*, 11–16.
- (53) Zhao, W.; An, L.; Wang, S. Recyclable high-performance epoxy-anhydride resins with DMP-30 as the catalyst of transesterification reactions. *Polymers* **2021**, *13*, 1–18.
- (54) Tran, T.-N.; Mauro, C. Di.; Grailot, A.; Mija, A. Chemical Reactivity and the Influence of Initiators on the Epoxidized Vegetable Oil/Dicarboxylic Acid System. *Macromolecules* **2020**, *53*, 2526–2538.
- (55) M, T.; E, J. HR-MAS NMR Spectroscopy in Material Science. In *Advanced Aspects of Spectroscopy*; INTECH, 2012 DOI: [10.5772/48340](https://doi.org/10.5772/48340).